Micro and Nanostructures 163 (2022) 107128

Contents lists available at ScienceDirect

Micro and Nanostructures

journal homepage: www.journals.elsevier.com/micro-and-nanostructures

Enhanced hole concentration in strain-compensated BAlN/AlGaN superlattice for deep ultraviolet light-emitting diodes

Wen Gu[a,b], Yi Lu[a], Zhiyuan Liu[a], Che-Hao Liao[a], Jianchang Yan[b,*], Junxi Wang[b], Jinmin Li[b], Xiaohang Li[a,**]

[a] Advanced Semiconductor Laboratory, King Abdullah University of Science and Technology, Thuwal, 23955-6900, Saudi Arabia
[b] Research and Development Center for Solid State Lighting, Institute of Semiconductors, Chinese Academy of Sciences, Beijing, 100083, China

ARTICLE INFO

Keywords:
Light-emitting diodes (LEDs)
BAlN
Superlattice
Hole concentration

ABSTRACT

The hole concentration in the strain-compensated $B_{0.14}Al_{0.86}N/Al_{0.5}Ga_{0.5}N$ superlattice (SCSL) is investigated. Compared with the $Al_{0.6}Ga_{0.4}N/Al_{0.5}Ga_{0.5}N$ SL, the effective hole concentration in the SCSL could be improved from 1.1×10^{17} cm^{-3} to 8.7×10^{18} cm^{-3} due to the remarkably enlarged valence band bending from 53 meV to 533 meV. We then propose the ultraviolet light-emitting diode (UV LED) structure emitting at 284 nm with the SCSL p-region. Compared with the bulk p-region structure, the UV LED with the SCSL p-region shows improved output characteristics due to the reduced electron leakage and improved hole injection ability. The internal quantum efficiency (IQE) and droop ratio of the SCSL LED structure increases from 49.5% to 54.1% and decreases from 36.8% to 13.6%, respectively. Moreover, the light output powers of the $Al_{0.6}Ga_{0.4}N/Al_{0.5}Ga_{0.5}N$ SL structure and SCSL structure have been improved by 16.3% and 49.1% over the bulk p-region counterpart. Our results indicate that the SCSL structure can be a promising candidate for the high-performance UV LED.

1. Introduction

Effective p-type doping of AlGaN films is of great importance for deep ultraviolet light-emitting diode (DUV LED). However, the conductivity of AlGaN films is poor for that the acceptor (eg: Mg) activation energy is extremely large in the high-Al composition AlGaN films, for example, the Mg activation energy in GaN and AlN films are 170 and 500 meV, respectively [1,2]. The generally adopted p-type AlGaN films cannot activate enough holes to combine with electrons in the active region, resulting in the increase of resistance and low radiative recombination efficiency of LED. Moreover, the AlGaN films grown on the AlN template suffer from compressive stress because of the lattice mismatch between AlN and GaN (2.5% [3]). The compressive stress could induce misfit dislocations and lead to crack generation during the epitaxy and deteriorate the output properties of LED [4,5]. To thoroughly develop the potential of light-emitting devices, the highly conductive p-type AlGaN films with less strain relaxation are highly desired.

Superlattice (SL) has been proposed to effectively improve the conductivity of p-type AlGaN films because of the spontaneous and piezoelectric field-induced energy shift of the valence band [6,7]. The Mg-doped $AlN/Al_{0.75}Ga_{0.25}N$ SL and $Al_{0.63}Ga_{0.37}N/Al_{0.51}Ga_{0.49}N$ SL with the hole concentration on the order of 10^{18} cm^{-3} have been demonstrated [8,9]. Moreover, strain-compensated superlattice (SCSL), such as the p-type AlGaN/InGaN SCSL, has been proposed to improve the performance of (In)GaN-based LEDs [10,11]. Due to

* Corresponding author.
** Corresponding author.
E-mail addresses: yanjc@semi.ac.cn (J. Yan), xiaohang.li@kaust.edu.sa (X. Li).

https://doi.org/10.1016/j.spmi.2021.107128
Received 7 October 2021; Received in revised form 14 November 2021; Accepted 22 December 2021
Available online 23 December 2021

that, the lattice constant of AlGaN and InGaN are smaller and larger than that of GaN, respectively, the strain of the AlGaN/InGaN SL grown on the GaN template could be fully compensated. As a result, the crack generation could be suppressed, and the crystal quality of epitaxial films could be improved. However, this AlGaN/InGaN SCSL could not be used in the DUV LED due to the ultraviolet light absorption of the InGaN material. Besides, to compensate for the compressive stress of AlGaN films grown on the AlN template, the employment of InGaN material will be out of efficiency due to the large lattice constant.

Wurtzite BAlN alloys possess unique properties in polarization and strain modulation are promising to be used in UV LED and high electron mobility transistors (HEMTs) [12,13]. In our recent work, the band alignment of BAlN/AlGaN heterostructures has been investigated experimentally, revealing the device applications of BAlN alloys [14,15]. Moreover, the multiple-pairs $B_xAl_{1-x}N$/AlN and $B_{0.14}Al_{0.86}N/Al_{0.7}Ga_{0.3}N$ SL structures have been demonstrated [16,17]. Furthermore, the a-lattice and c-lattice constant of $B_{0.14}Al_{0.86}N$ have been reported to be 3.027 and 4.798 Å, respectively [18]. The value of the a-lattice constant of $B_{0.14}Al_{0.86}N$ is smaller than that of AlN (3.112 Å [19]), implying that the $B_{0.14}Al_{0.86}N$ films grown on the AlN template will be under tensile stress. The opposite stress state of $B_{0.14}Al_{0.86}N$ and AlGaN films on the AlN template has also been observed by scanning transmission electron microscopy (STEM) measurements [17]. As a result, the periodically grown $B_{0.14}Al_{0.86}N$ and AlGaN films on the AlN template could effectively reduce the overall stress of the SL structure. In this study, the hole concentration enhancement at the interface of the strain-compensated $B_{0.14}Al_{0.86}N/Al_{0.5}Ga_{0.5}N$ SL is theoretically investigated. The replacement of the conventional $Al_{0.5}Ga_{0.5}N$ p-region with the $Al_{0.6}Ga_{0.4}N/Al_{0.5}Ga_{0.5}N$ SL p-region and SCSL p-region in the UV LED structure emitting at 284 nm is also carried out. The energy band profiles, carrier distributions, and output characteristics of these LEDs are systematically presented.

2. Strain-compensated superlattice (SCSL)

The strain of an epitaxial layer grown on substrate considering the lattice constant difference is defined as equation [20]. a_{sub} and a_{epi} are the lattice constant of the substrate and epitaxial layer, respectively. When applying the strain calculation method to design the SCSL, the thickness and lattice constant of each layer of the SL should be taken into consideration. The average a-lattice constant of the SCSL ($< a >$) is described as equation (2) [20]. t_1, t_2 and a_1, a_2 are the thickness and unstrained lattice constant of each layer. For the SCSL, the average stain should be zero, meaning that the value of $< a >$ is equal to the value of a_{sub}.

$$\varepsilon = \frac{a_{sub} - a_{epi}}{a_{epi}} \tag{1}$$

$$< a > = \frac{t_1 a_1 + t_2 a_2}{t_1 + t_2} \tag{2}$$

In this work, the proposed SCSL is grown on the AlN/sapphire template (a_{sub} =3.112 Å [19]). The thickness of the $B_{0.14}Al_{0.86}N$ film is assumed to be 2 nm (a_1 =3.027 Å [18], t_1 = 2 nm). To compensate for the strain of the $B_{0.14}Al_{0.86}N$ film, the thickness and composition of the $Al_xGa_{1-x}N$ film can be modulated by the employment of Vegard's Law. The composition of the AlGaN film is chosen to be 50%. The lattice constant of $Al_{0.5}Ga_{0.5}N$ is 3.151 Å, which is calculated by Vegard's Law, and the calculated compensating thickness is 4 nm (a_2 =3.151 Å, t_2 = 4 nm). As the highly p-type doping is hardly achieved in the high Al composition AlGaN films, we adopt the $Al_{0.6}Ga_{0.4}N$ films (a_3 =3.143 Å) with the same thickness as $B_{0.14}Al_{0.86}N$ films as a reference superlattice structure.

The number of holes at the interface of the superlattice is determined by the magnitude of the band bending (ΔV_B) [21], [22]. The energy band diagrams of the $Al_{0.6}Ga_{0.4}N/Al_{0.5}Ga_{0.5}N$ SL and SCSL are shown in Fig. 1a and Fig. 1c. Due to the large polarization field of $B_{0.14}Al_{0.86}N$ material, the ΔV_B of SCSL (ΔV_B = 533 meV) is distinctly larger than that of $Al_{0.6}Ga_{0.4}N/Al_{0.5}Ga_{0.5}N$ SL (ΔV_B = 53 meV). Moreover, the position of the valence band of SCSL is higher than the Fermi Level (E_F), indicating that the number of holes at the interface will be extremely high. The simulated hole concentrations of these two kinds of superlattice are shown in Fig. 1b and d. The peak hole concentration at the interface of the $Al_{0.6}Ga_{0.4}N/Al_{0.5}Ga_{0.5}N$ SL and SCSL are around 4.0×10^{17} cm^{-3} and 1.5×10^{20} cm^{-3}, respectively. Moreover, holes are more confined with less broadened peaks in the SCSL due to the large valence band difference between $B_{0.14}Al_{0.86}N$ and $Al_{0.5}Ga_{0.5}N$. The effective hole concentration in each pair of the SL is defined as the arithmetic average over one period of the SL [22]. The calculated effective hole concentration in the $Al_{0.6}Ga_{0.4}N/Al_{0.5}Ga_{0.5}N$ SL and SCSL are 1.1×10^{17} cm^{-3} and 8.7×10^{18} cm^{-3}, respectively. It is worth mentioning that the effective hole concentration of the SCSL is almost two orders of magnitude greater than that of the $Al_{0.6}Ga_{0.4}N/Al_{0.5}Ga_{0.5}N$ SL. Such a $B_{0.14}Al_{0.86}N/Al_{0.5}Ga_{0.5}N$ structure is beneficial to both the stress compensation and hole concentration enhancement, which is excellent to be the hole injection layer of UV LED.

3. DUV LEDs with BAlN/AlGaN superlattice

The schematic diagrams of the designed UV LED structures are shown in Fig. 2. The conventional structure (LED A) is grown on an AlN/sapphire template. The 3-μm Si-doped $Al_{0.5}Ga_{0.5}N$ cladding layer (n-doping = 5×10^{18} cm^{-3}) is deposited firstly. The active region is composed of five 2-nm $Al_{0.4}Ga_{0.6}N$ quantum wells (QWs) sandwiched by six 12-nm $Al_{0.5}Ga_{0.5}N$ quantum barriers (QBs). Above the last QB, the 10-nm Mg-doped $Al_{0.65}Ga_{0.45}N$ (p-doping = 2×10^{19} cm^{-3}) electron-blocking layer (EBL), 24-nm Mg-doped $Al_{0.5}Ga_{0.5}N$ (p-doping = 2×10^{19} cm^{-3}) hole injection layer and 10-nm Mg-doped GaN (p-doping = 1×10^{20} cm^{-3}) cap layer are deposited sequentially. In this study, we employ two kinds of superlattice hole injection layers. For the LED B, the hole injection layer is replaced by the 4-pairs 2-nm $Al_{0.6}Ga_{0.4}N$/4-nm $Al_{0.5}Ga_{0.5}N$ SL, while the 4-pairs 2-nm $B_{0.14}Al_{0.86}N$/4-nm $Al_{0.5}Ga_{0.5}N$ SCSL is adopted in the LED

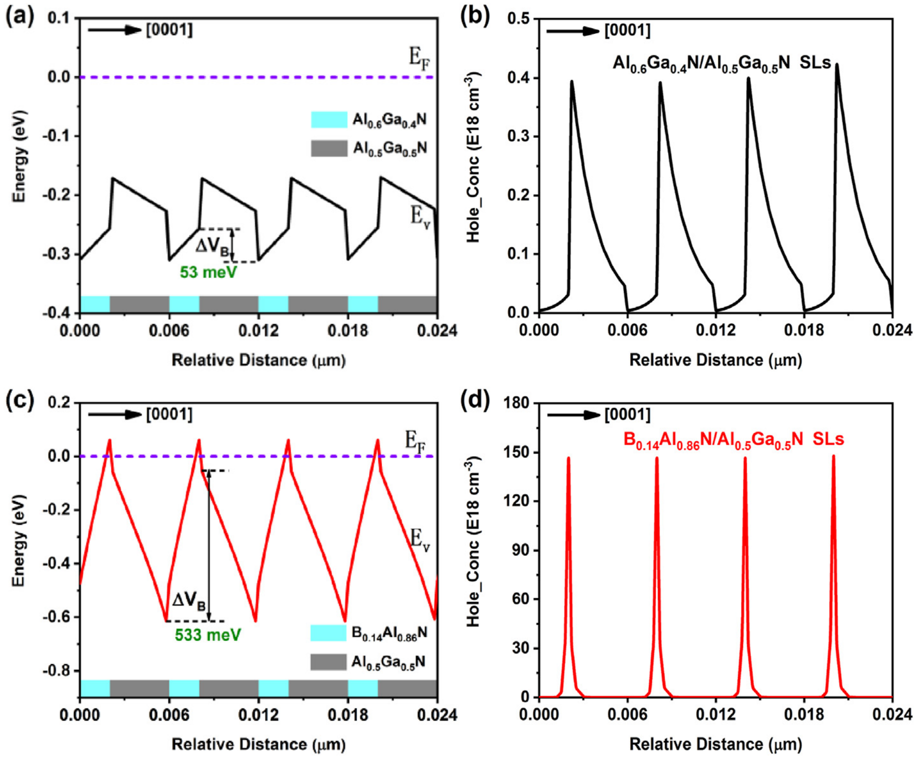

Fig. 1. (a) Energy band diagram of $Al_{0.6}Ga_{0.4}N/Al_{0.5}Ga_{0.5}N$ SLs, (b) hole concentration of $Al_{0.6}Ga_{0.4}N/Al_{0.5}Ga_{0.5}N$ SLs, (c) energy band diagram of $B_{0.14}Al_{0.86}N/Al_{0.5}Ga_{0.5}N$ SLs, and (d) hole concentration of $B_{0.14}Al_{0.86}N/Al_{0.5}Ga_{0.5}N$ SLs at equilibrium. All the parameters including the doping concentration, acceptor activation energy, and polarization screening factor are the same as the LED structures in the part of DUV LEDs with BAlN/AlGaN superlattice.

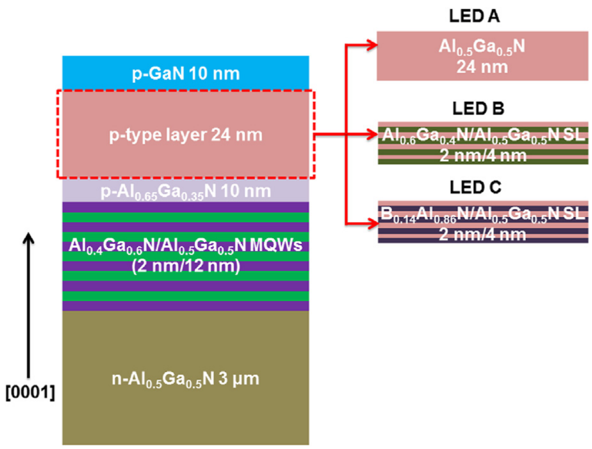

Fig. 2. Schematic diagrams of UV LEDs with different p-type layers. LED A is the conventional structure with a p-type $Al_{0.5}Ga_{0.5}N$ layer. LED B has the p-type $Al_{0.6}Ga_{0.4}N/Al_{0.5}Ga_{0.5}N$ SLs and LED C has the strain-compensated p-type $B_{0.14}Al_{0.86}N/Al_{0.5}Ga_{0.5}N$ SLs.

C. The total thickness and Mg doping concentration of these hole injection layers in the three LEDs are kept equal. Other layers of LED B and C are kept the same as LED A.

The simulation software used in this study is the Advanced Physical Models of Semiconductor Devices (APSYS) program. The band offset ratio of AlGaN materials is set to be 0.7/0.3 [23]. The bandgap of AlGaN film is calculated by formula (3), with a bowing parameter b of 0.94 [24]. The polarization constants (including spontaneous polarization (SP) and piezoelectric (PZ) constants) of AlGaN materials can be found in Ref. [25]. The mobility and effective mass of carriers in the AlGaN materials are the generally accepted values from the experimental results [23]. The acceptor activation energy of the AlGaN films increases linearly with the Al composition [1,2]. The bandgap of $B_{0.14}Al_{0.86}N$ is set to be 5.7 eV, which is calculated by first-principles calculation based on density functional

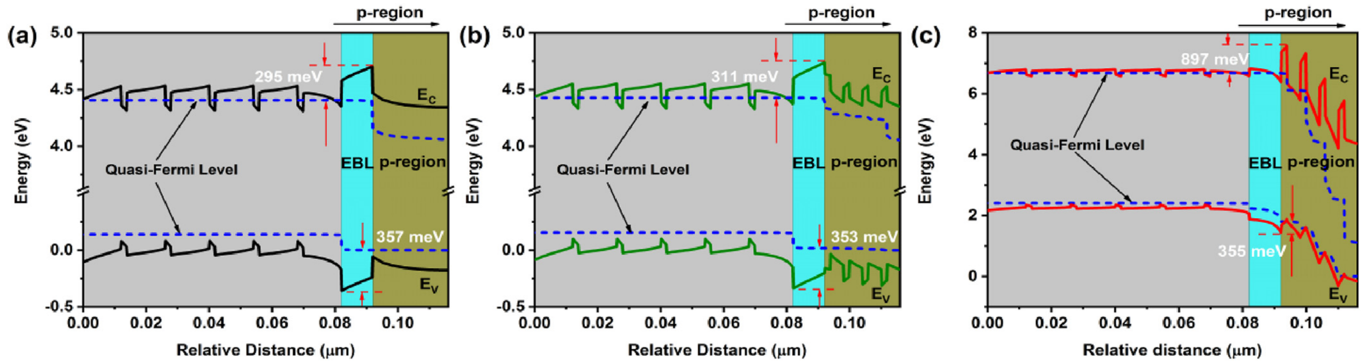

Fig. 3. Energy band diagrams of (a) LED A, (b) LED B, and (c) LED C at 75 mA.

theory (DFT) [18]. The acceptor activation energy of the $B_{0.14}Al_{0.86}N$ material is set to be 170 meV due to the similar valence band edge of $B_{0.14}Al_{0.86}N$ and GaN [14]. The conduction and valence band edges of $B_{0.14}Al_{0.86}N$ are 1.3 eV and 0.1 eV higher than that of $Al_{0.5}Ga_{0.5}N$ [14,15]. Moreover, the detailed parameters of $B_{0.14}Al_{0.86}N$ materials can be found in our previous work [12,26].

$$E_g(Al_xGa_{1-x}N) = xE_g(AlN) + (1-x)E_g(GaN) - bx(1-x) \tag{3}$$

The Auger recombination coefficient, Shockley-Read-Hall (SRH) recombination lifetime, and radiative recombination rate can be found in our previous work [12]. The light-extraction efficiency is set to be 10% [27]. The background loss and operating temperature are assumed to be 2000 m^{-1} and 300 K [12], respectively. Considering the polarization screening effect of the defect, the polarization level is set to be 40% for our designed structures [28].

Fig. 3 shows the energy band diagrams and quasi-Fermi levels of LED A, B, and C at 75 mA, respectively. The energy bands at the last QB of these LED structures are pulled down due to the polarization electric field. To evaluate the capability in blocking electrons and promoting hole injection of these LED structures, the effective barrier heights of electron (Φ_e) and hole (Φ_h) are calculated. The values of Φ_e for LED A, B, and C are 295, 311, and 897 meV, respectively. The large Φ_e value of LED C is attributed to the large bandgap of BAlN material and the band alignment of BAlN/AlGaN property, which has also been reported in our previous work [12]. The larger Φ_e of LED B and C implies that the suppression of electron overflow could be improved by the employment of the SL structure, especially the SCSL structure. The values of Φ_h for LED A, B, and C are 357, 353, and 355 meV, respectively. The slightly reduced Φ_h could be favorable for the hole injection from the p-region to the active region. In terms of these values of Φ_e and Φ_h, it could be found that the SCSL p-region has a great effect on the Φ_e, but the inconspicuous impact on the Φ_h compared with the bulk $Al_{0.5}Ga_{0.5}N$ or $Al_{0.6}Ga_{0.4}N/Al_{0.5}Ga_{0.5}N$ SL p-region.

The electron current density (ECD) and hole current density (HCD) of these LED structures at 75 mA are shown in Fig. 4. The ECD in the p-region of LED A, B, and C are 46.3, 31.5, and near 0 A/cm^2, respectively. The much lower ECD in the p-region of LED C indicates that the electron leakage of LED C is the lowest. The reason for the superiority of LED C in hindering electron overflow could be attributed to the higher effective barrier height of electrons in the SCSL structures. The less electron leakage will be beneficial for the reduction of nonradiative recombination in the p-region. The HCD in the p-region of LED A, B, and C are 78.7, 93.5, and 125.0 A/cm^2, respectively. The hole injection ability of LED C is the best among these LED structures. The enhanced hole injection efficiency of LED C could be explained by the fact that the supplied holes from the p-region could be greatly promoted by the employment of the SCSL structure.

The electron concentration, hole concentration, and radiative recombination rate in the active region of these LED structures at 75 mA are shown in Fig. 5. The highest electron and hole concentration, as well as radiative recombination rate are obtained in LED C. On the one hand, LED B and C have larger effective barrier heights of electron (as shown in Fig. 3), which could effectively block the electron overflow to the p-region. Thus, the electron concentrations in the active region of LED B and C are higher than LED A. On the other hand, the SL hole injection layer of LED B and C could activate more holes than LED A, especially the SCSL (as shown in Fig. 1). Therefore, the hole concentration in the active regions of LED B and C could also be improved even though the effective barrier height of hole is comparable in these LED structures. The peak radiative recombination rate of LED C and LED B are 5.0×10^{26} and 4.0×10^{26} cm^{-3}/s, which are 1.5 and 1.2 times that of LED A (3.4×10^{26} cm^{-3}/s), respectively. The enhancement of the radiative recombination rate of LED B and C could be attributed to the improvement of electron and hole concentrations in the active region.

The internal quantum efficiency (IQE), output power, I–V characteristics, and wall-plug efficiency (WPE) of these LED structures at the current of 75 mA are shown in Fig. 6. For the LED C, the peak efficiency can be achieved to be 54.1%, while those values of LED A and LED B are 49.5% and 50.4%. The droop ratio of LED C is 13.6%, which is much lower than those values of LED A (36.8%) and LED B (27.6%). One reason is that the higher electron barrier height of LED C blocks electron overflow to p-region, as shown in Fig. 3. The resultant lower electron current leakage will lead to a higher current at 75 mA, and less droop. When comparing LED A and LED B, the efficiency drop of LED B is still lower than LED A, although they have similar effective electron and hole barrier heights. This is because

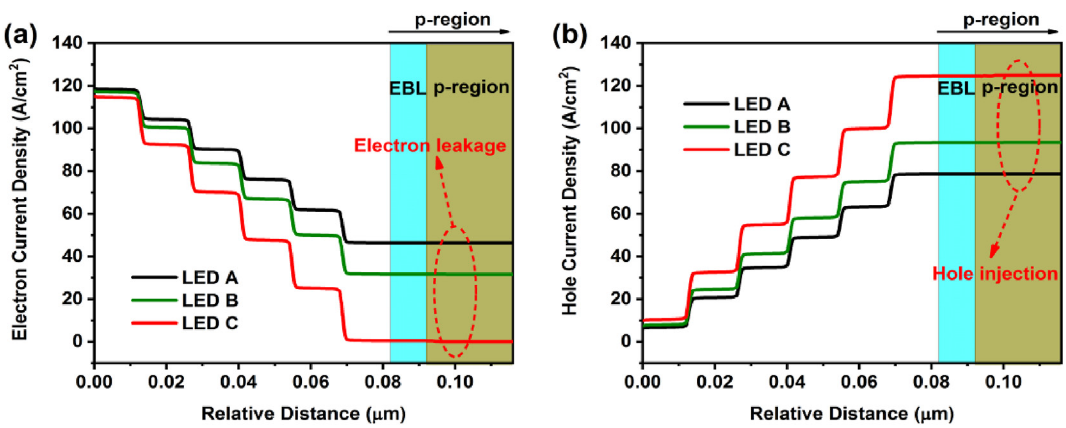

Fig. 4. (a) Electron, and (b) hole current density of LED A, B, and C at 75 mA.

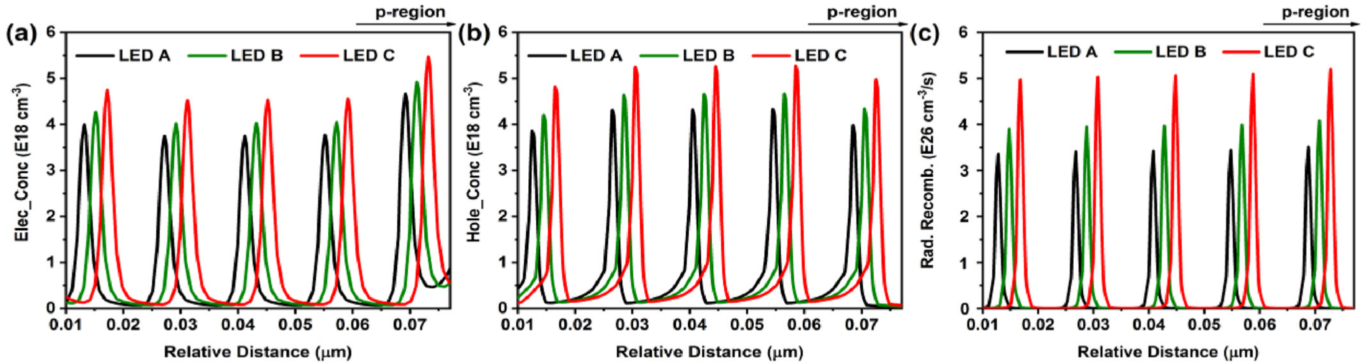

Fig. 5. (a) Electron concentration, (b) hole concentration, and (c) radiative recombination rate of LED A, B, and C at 75 mA. For better comparison, the position of the green and red lines are right-shifted by 2 nm and 4 nm, respectively.

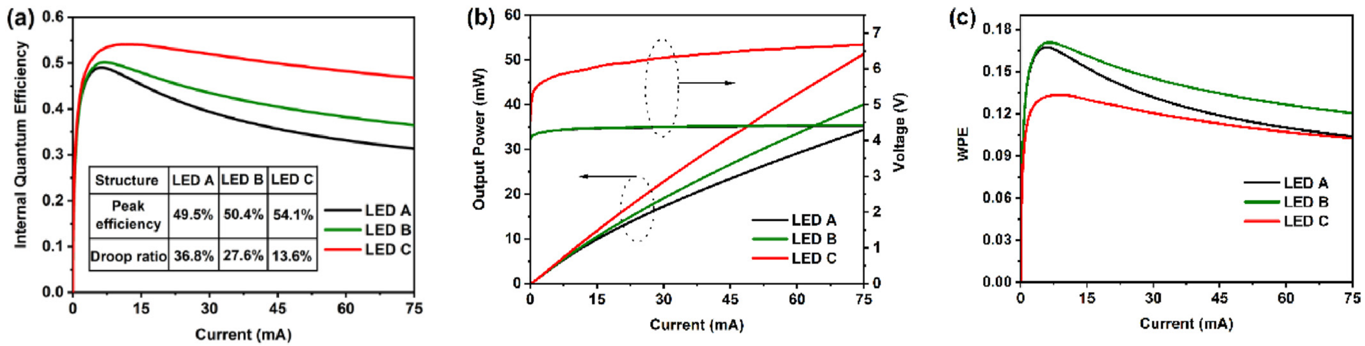

Fig. 6. (a) IQE, and (b) output power and I–V characteristics of LED A, B, and C at 75 mA.

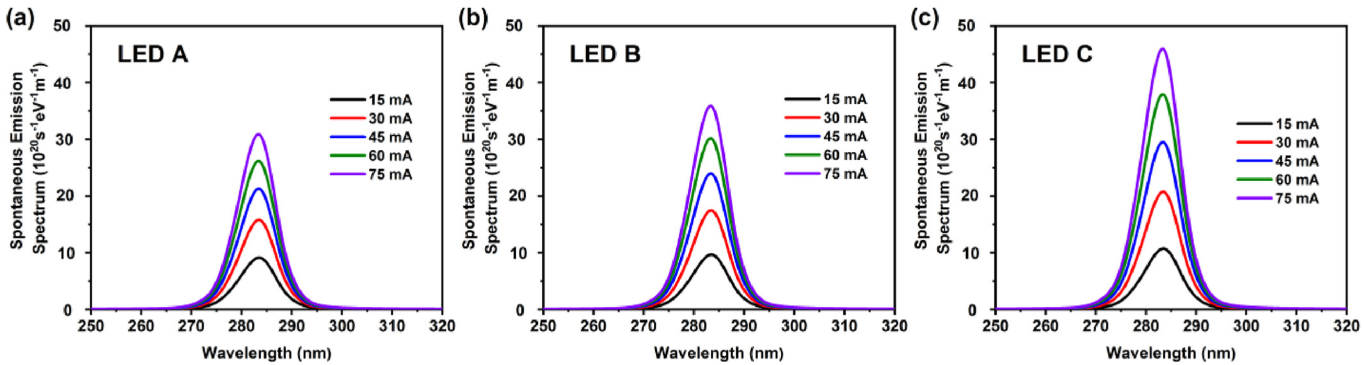

Fig. 7. The spontaneous emission spectrum of (a) LED A, (b) LED B, and (c) LED C at 15, 30, 45, 60, 75 mA.

the more holes activated by the superlattice p-region, which is verified by the hole concentration in the QWs, as shown in Fig. 5. In this aspect, the effective hole concentration in the BAlN/AlGaN SCSL (8.7×10^{18} cm^{-3}) is almost two orders of magnitude greater than that of AlGaN/AlGaN SL (1.1×10^{17} cm^{-3}), as shown in Fig. 1. Thus, the droop ratio of LED C is remarkably reduced compared with LED A and LED B.

The output power of LED A, B, and C are 34.4 mW, 40.0 mW, and 51.3 mW, respectively. Compared with LED A, the output power of LED B and C has been improved by 16.3% and 49.1%. The output power enhancement of LED C could be attributed to the greatly reduced electron leakage and improved hole injection by using the SCSL. The I–V characteristics of LED A and LED B are almost the same, indicating the $Al_{0.6}Ga_{0.4}N/Al_{0.5}Ga_{0.5}N$ superlattice p-region has less effect on the I–V characteristics of LED due to the similar conduction and valence band edge profiles of $Al_{0.6}Ga_{0.4}N$ and $Al_{0.5}Ga_{0.5}N$, as shown in Fig. 3a and b. However, LED C shows a larger turn-on voltage (5.84 V), which is defined as the intersection of voltage and the slope of the linear part of the I–V curve, than the values of the LED A (4.32 V) and LED B (4.34 V). It is due to the quite large Φ_e in LED C, which seriously hinders the flow of electrons, as shown in Fig. 3c.

The WPE, which is defined as the ratio of output power to the input electrical power, as shown in Fig. 6c. LED B has the highest WPE, while LED C shows the lowest value. It is because of LED C shows the highest turn-on voltage, as shown in Fig. 6b. However, when the LED works at high injection current, the WPE shows less difference. It means the energy consumption will not so severe at this circumstance. One way to improve the WPE of LED C is to reduce the pairs of superlattice, but it will weaken the superiority of superlattice in hole generation and blocking electrons. The coordination of the work efficiency and energy consumption should be taken into consideration in the future. Although the WPE of LED C is worse than LED A and LED B, it is still worth noticing that the efficiency, output power, and radiative recombination rate of LED C are the best among these LED structures. Moreover, the BAlN/AlGaN SL is a strain compensated structure, which will be beneficial for the future epitaxy demonstration, such as crack-free. Furthermore, the BAlN material is also the first and only choice to design the strain-compensated superlattice for deep UV LEDs.

The spontaneous emission spectrums of these LED structures are shown in Fig. 7. Single peaks with the emission peak wavelength of 284 nm are observed in these structures, indicating that our SCSLs structure has a negligible effect on the emission wavelength. LED C shows the highest spontaneous emission rate due to the highest radiative recombination rate in the active region, as shown in Fig. 5c. These results mean that the emission property of UV LEDs can be remarkably improved by using the SCSL structure.

4. Conclusion

We have built the BAlN based SCSL structure and analyzed the mechanism of hole concentration enhancement in the SCSL. Because of the large valence band bending, the achieved effective hole concentration in the SCSL can be as high as 8.7×10^{18} cm^{-3}. We then design three UV LED structures with different p-regions, which are bulk $Al_{0.5}Ga_{0.5}N$, $Al_{0.6}Ga_{0.4}N/Al_{0.5}Ga_{0.5}N$ SL, and SCSL, respectively. It can be observed that the effective barrier height of the electron increases by using the SL structure, and even more apparent in the SCSL. This phenomenon could be one reason for the reduced electron leakage in the LED structure with the SCSL p-region. Although the effective barrier height of the hole is comparable among these structures, the hole injection ability of the LED structure with SCSL p-region still increases remarkably on account of the more activated holes in the SCSL p-region. Therefore, the carrier concentrations and radiative recombination rate in the active region of the UV LED with SCSL p-region are increased compared with the reference structures. The efficiency droop ratio of the UV LED with SCSL p-region is significantly reduced from 36.8% (bulk p-region structure) to 13.6% (SCSL p-region structure). The output power of the UV LED with SCSL p-region can reach 51.3 mW. This structure provides a new view to design the high-performance UV LED.

Credit author statement

Wen Gu: Writing – original draft, Conceptualization, Methodology, Data curation, Formal analysis, Investigation. **Yi Lu**: Investigation, Writing – review & editing, Methodology, Formal analysis. **Zhiyuan Liu**: Investigation, Writing – review & editing. **Che-Hao Liao**: Investigation, Writing – review & editing. **Jianchang Yan**: Supervision, Resources, Funding acquisition, Validation, Investigation. **Junxi Wang**: Investigation, Supervision, Funding acquisition. **Jinmin Li**: Supervision, Validation, Formal analysis, Investigation, Data curation. **Xiaohang Li**: Supervision, Resources, Funding acquisition, Validation, Formal analysis, Investigation, Data curation.

Declaration of competing interest

On behalf of all authors, the corresponding author states that there is no conflict of interest.

Acknowledgments

The KAUST authors acknowledge the support of KAUST Baseline Fund BAS/1/1664-01-01, GCC Research Council Grant REP/1/3189-01-01, and Competitive Research Grants URF/1/3437-01-01 and URF/1/3771-01-01. The authors of Institute of Semiconductors acknowledge the support of the National Key R&D Program of China (Nos. 2016YFB0400800), the National Natural Sciences Foundation of China (Grant Nos. 62022080, 61904176), Beijing Nova Program Z181100006218007, Shanxi Key R&D Program 20201102013.

References

[1] W. Götz, N.M. Johnson, J. Walker, D.P. Bour, R.A. Street, Activation of acceptors in Mg-doped GaN grown by metalorganic chemical vapor deposition, Appl. Phys. Lett. 68 (5) (Jan. 1996) 667–669, https://doi.org/10.1063/1.116503.

[2] K.B. Nam, M.L. Nakarmi, J. Li, J.Y. Lin, H.X. Jiang, Mg acceptor level in AlN probed by deep ultraviolet photoluminescence, Appl. Phys. Lett. 83 (5) (Aug. 2003) 878–880, https://doi.org/10.1063/1.1594833.

[3] A.F. Wright, J.S. Nelson, Consistent structural properties for AlN, GaN, and InN, Phys. Rev. B 51 (12) (Mar. 1995) 7866–7869, https://doi.org/10.1103/PhysRevB.51.7866.

[4] P. Dong, et al., AlGaN-based deep ultraviolet light-emitting diodes grown on nano-patterned sapphire substrates with significant improvement in internal quantum efficiency, J. Cryst. Growth 395 (Jun. 2014) 9–13, https://doi.org/10.1016/j.jcrysgro.2014.02.039.

[5] X. Chen, et al., Effect of AlN buffer on the properties of AlN films grown on sapphire substrate by MOCVD, in: SSLChina, IFWS, Beijing, China, Nov. 2016, pp. 123–126, https://doi.org/10.1109/IFWS.2016.7803774.

[6] P. Kozodoy, M. Hansen, S.P. DenBaars, U.K. Mishra, Enhanced Mg doping efficiency in $Al_{0.2}Ga_{0.8}N$/GaN superlattices, Appl. Phys. Lett. 74 (24) (Jun. 1999) 3681–3683, https://doi.org/10.1063/1.123220.

[7] K. Kumakura, T. Makimoto, N. Kobayashi, Enhanced hole generation in Mg-doped AlGaN/GaN superlattices due to piezoelectric field, Jpn. J. Appl. Phys. 39 (4B) (Apr. 2000) 2428–2430, https://doi.org/10.1143/JJAP.39.2428.

[8] K. Ebata, J. Nishinaka, Y. Taniyasu, K. Kumakura, High hole concentration in Mg-doped AlN/AlGaN superlattices with high Al content, Jpn. J. Appl. Phys. 57 (4S) (Mar. 2018), 04FH09, https://doi.org/10.7567/JJAP.57.04FH09.

[9] T.C. Zheng, et al., Improved p-type conductivity in Al-rich AlGaN using multidimensional Mg-doped superlattices, Sci. Rep. 6 (1) (Feb. 2016) 1–10, https://doi.org/10.1038/srep21897.

[10] J.Y. Xiong, et al., Advantages of GaN based light-emitting diodes with p-AlGaN/InGaN superlattice last quantum barrier, Opt Commun. 312 (Feb. 2014) 85–88, https://doi.org/10.1016/j.optcom.2013.08.053.

[11] F.M. Chen, et al., Numerical analysis of using superlattice-AlGaN/InGaN as electron blocking layer in green InGaN light-emitting diodes, in: Proc. SPIE, San Francisco, CA, USA vol. 8625, Mar. 2013, p. 862526, https://doi.org/10.1117/12.2003681.

[12] W. Gu, et al., BAlN for III-nitride UV light-emitting diodes: undoped electron blocking layer, J. Phys. D Appl. Phys. 54 (17) (Feb. 2021) 175104, https://doi.org/10.1088/1361-6463/abdefc.

[13] R. Lin, et al., BAlN alloy for enhanced two-dimensional electron gas characteristics of GaN/AlGaN heterostructures, J. Phys. D Appl. Phys. 53 (48) (Sep. 2020) 48LT01, https://doi.org/10.1088/1361-6463/aba4d5.

[14] H. Sun, et al., Nearly-zero valence band and large conduction band offset at BAlN/GaN heterointerface for optical and power device application, Appl. Surf. Sci. 458 (Jul. 2018) 949–953, https://doi.org/10.1016/j.apsusc.2018.07.178.

[15] H. Sun, et al., Band alignment of $B_{0.14}Al_{0.86}N/Al_{0.7}Ga_{0.3}N$ heterojunction, Appl. Phys. Lett. 111 (12) (Sep. 2017) 122106, https://doi.org/10.1063/1.4999249.

[16] M. Abid, et al., Distributed Bragg reflectors based on diluted boron-based BAlN alloys for deep ultraviolet optoelectronic applications, Appl. Phys. Lett. 100 (5) (Jan. 2012), 051101, https://doi.org/10.1063/1.3679703.

[17] H. Sun, et al., Revealing microstructure and dislocation behavior in BAlN/AlGaN heterostructures, APEX 11 (1) (Dec. 2017), 011001, https://doi.org/10.7567/APEX.11.011001.

[18] M. Zhang, X. Li, Structural and electronic properties of wurtzite $B_xAl_{1-x}N$ from first-principles calculations, Phys. Status Solidi B 254 (8) (Jun. 2017) 1600749, https://doi.org/10.1002/pssb.201600749.

[19] W.M. Yim, et al., Epitaxially grown AlN and its optical band gap, J. Appl. Phys. 44 (1) (Jan. 1973) 292–296, https://doi.org/10.1063/1.1661876.

[20] R.W. Enck, et al., Plasma-assisted molecular beam epitaxy of strain-compensated a-plane InGaN/AlGaN superlattices, Phys. Status Solidi C 12 (4–5) (Jan. 2015) 434–438, https://doi.org/10.1002/pssc.201400208.

[21] E.F. Schubert, W. Grieshaber, I.D. Goepfert, Enhancement of deep acceptor activation in semiconductors by superlattice doping, Appl. Phys. Lett. 69 (24) (Oct. 1996) 3737–3739, https://doi.org/10.1063/1.117206.

[22] I.D. Goepfert, E.F. Schubert, A. Osinsky, P.E. Norris, N.N. Faleev, Experimental and theoretical study of acceptor activation and transport properties in p-type $Al_xGa_{1-x}N$/GaN superlattices, J. Appl. Phys. 88 (4) (May 2000) 2030–2038, https://doi.org/10.1063/1.1305842.

[23] I. Vurgaftman, J.N. Meyer, Band parameters for nitrogen-containing semiconductors, J. Appl. Phys. 94 (6) (Sep. 2003) 3675–3696, https://doi.org/10.1063/1.1600519.

[24] C. Coughlan, S. Schulz, M.A. Caro, E.P. O'Reilly, Band gap bowing and optical polarization switching in AlGaN alloys, Phys. Status Solidi B 252 (5) (Jan. 2015) 879–884, https://doi.org/10.1002/pssb.201451593.

[25] K. Liu, X. Li, Polarization Properties of Wurtzite III Nitride Indicate the Principle of Polarization Engineering, Aug. 2018 arXiv preprint arXiv:1808.07211.

[26] K. Liu, et al., Wurtzite BAlN and BGaN alloys for heterointerface polarization engineering, Appl. Phys. Lett. 111 (22) (Nov. 2017) 222106, https://doi.org/10.1063/1.5008451.

[27] Z. Ren, et al., III-nitride deep UV LED without electron blocking layer, IEEE Photonics J. 11 (2) (Apr. 2019) 8200511, https://doi.org/10.1109/JPHOT.2019.2902125.

[28] Z.H. Zhang, et al., Nearly efficiency-droop-free AlGaN-based ultraviolet light-emitting diodes with a specifically designed superlattice p-type electron blocking layer for high Mg doping efficiency, Nanoscale Res. Lett. 13 (1) (Apr. 2018) 1–7, https://doi.org/10.1186/s11671-018-2539-9.